*inorganics*

MDPI

*Article*

# Polymeric Copper(II) Complexes with a Newly Synthesized Biphenyldicarboxylic Acid Schiff Base Ligand—Synthesis, Structural and Thermal Characterization

**Milica G. Bogdanović, Nikola D. Radnović, Berta Barta Holló *, Mirjana M. Radanović, Branko B. Kordić, Vidak N. Raičević, Ljiljana S. Vojinović-Ješić and Marko V. Rodić**

Faculty of Sciences, University of Novi Sad, Trg Dositeja Obradovića 3, 21000 Novi Sad, Serbia
* Correspondence: berta.hollo@dh.uns.ac.rs

**Abstract:** The newly synthesized biphenyldicarboxylic acid Schiff base and its complexes with Cu(II) were synthesized, and their spectroscopic and structural analysis was performed. The reaction of the ligand and copper(II) acetate in different solvents resulted in the formation of two solvatomorphic complexes, one with MeOH, and the other with DMF molecules, in the crystal lattice. The differences in the results of the thermal analysis could be explained by the different polarities of the solvents present. SC-XRD analysis revealed that the ligand is coordinated as a dianion, in a pentadentate manner, through two phenoxide oxygen atoms, two azomethine nitrogen atoms, and with the oxygen atom of one carboxylate functioning as a bridge that connects the monomeric units. The coordination polyhedron was described with several parameters obtained from different methods of calculation. The presence of different solvents in the crystal structure results in differences in the H-bond networks, and an overall different crystal packing of the structural units in the obtained complexes.

**Keywords:** coordination polymer; copper(II); biphenydicarboxylic acid; Schiff base

check for updates

**Citation:** Bogdanović, M.G.; Radnović, N.D.; Barta Holló, B.; Radanović, M.M.; Kordić, B.B.; Raičević, V.N.; Vojinović-Ješić, L.S.; Rodić, M.V. Polymeric Copper(II) Complexes with a Newly Synthesized Biphenyldicarboxylic Acid Schiff Base Ligand—Synthesis, Structural and Thermal Characterization. *Inorganics* **2022**, *10*, 261. https://doi.org/10.3390/inorganics10120261

Academic Editor: Wolfgang Linert

Received: 10 November 2022
Accepted: 2 December 2022
Published: 16 December 2022

**Publisher's Note:** MDPI stays neutral with regard to jurisdictional claims in published maps and institutional affiliations.

**Copyright:** © 2022 by the authors. Licensee MDPI, Basel, Switzerland. This article is an open access article distributed under the terms and conditions of the Creative Commons Attribution (CC BY) license (https://creativecommons.org/licenses/by/4.0/).

## 1. Introduction

In recent years, coordination polymers (CPs) have become the focus of attention of numerous research groups because of their structural characteristics and topologies, as well as their various applications. The most important fields of potential applications are catalysis [1,2], luminescence [3], magnetism [4,5], gas storage [6], adsorption [7,8], etc. A great majority of the synthesized and characterized CPs contain *d*- and *f*-metals such as Ag, Zn, Cd, Fe, Mn, Cu, and lanthanides. Literature research has shown that some CPs containing Cu(II), Cu(I), and even mixed-valence CPs are promising due to their structural diversity, versatile application, and lower cost and toxicity in comparison with the abovementioned [9–11].

To obtain porous coordination polymers, dicarboxylates are very often used as ligands [8]. They can easily coordinate with the metal centers and form networks with a variety of properties. The dicarboxylates may be also modified to improve their adsorptive, catalytic, luminescent, and other properties. We opted to explore the condensation of salicylaldehyde with 2,2′-diamino-[1,1′-biphenyl]-4,4′-dicarboxylic acid, as the expected Schiff base product would have an increased number of potential donor atoms and hence an improved coordination ability of the dicarboxylate-type ligand, with an existing possibility of polymer formation. Schiff bases display a broad spectrum of useful properties, including a very good coordination ability toward metals [12,13]; their formation of coordination complexes with a variety of potential applications is also well-documented [14–17].

Schiff bases of amino-[1,1′-biphenyl]-dicarboxylic acids incorporating azomethine function coupled to the biphenyl ring system appear to be very rare. However, Schiff bases of [1,1′-biphenyl]-3,3′-dicarboxylic acid with 4-(1,2,2-triphenylethenyl)-benzaldehyde and 2-hydroxy-1-naphthaldehyde were patented as Diazomethine pigment dyes [18].

In addition, several polymeric Schiff bases of amino-[1,1′-biphenyl]-3,3′-dicarboxylic acid were synthesized [19]. There are limited reports of coordination compounds that include these compounds as ligands. These are obtained in post-synthetic modifications of DUT-5-based and UiO-67-based MOFs where salicylaldehyde or 2-formylpyridine were condensed with 2-amino-[1,1′-biphenyl]-4,4′-dicarboxylic acid [20–23] as well as post-synthetic modification of Zn(II) diperiodic coordination polymer where 4-(1,2,2-triphenylethenyl)-benzaldehyde was condensed with 4,4′-diamino-[1,1′-biphenyl]-2,2′-dicarboxylic acid [24].

In this paper, we report the synthesis, structure, and physical and chemical characterization of 2,2′-bis(((*E*)-2-hydroxybenzylidene)amino)-[1,1′-biphenyl]-4,4′-dicarboxylic acid and coordination polymers obtained by its reaction with Cu(II). In addition to the reaction conditions of the syntheses, the spectral and thermal characterization of the compounds is also presented here.

## 2. Results and Discussion

### *2.1. Syntheses of the Compounds*

The synthesis of 2,2′-diamino-[1,1′-biphenyl]-4,4′-dicarboxylic acid (**IV**) was achieved in a three-step synthetic pathway starting from the dimethyl ester of [1,1′-biphenyl]-4,4′-dicarboxylic acid (**I**) that entails nitration, reduction, and deprotection of the carboxylic acid, as shown in Scheme S1. The synthetic methodology is based on slightly modified literature procedures [25–27].

The one-step synthesis of ligand **$H_4$L** was achieved by the condensation of **IV** and salicylaldehyde in a 1:2 molar ratio in methanol with the formic acid present (Scheme 1). The ligand was obtained in good yield (82%). The $^1$H NMR spectrum features 10 signals, each corresponding to a pair of chemically equivalent protons. The exchangeable protons of the carboxylic acid groups appear as a broad signal at 13.29 ppm, upfield of which is a sharp singlet corresponding to protons of the phenol groups (12.23 ppm); the appearance of the phenol proton signal is indicative of an intramolecular hydrogen bond. Resonances of the aromatic-ring carbon and hydrogen nuclei were assigned with the aid of 2D NMR techniques (Figure S6).

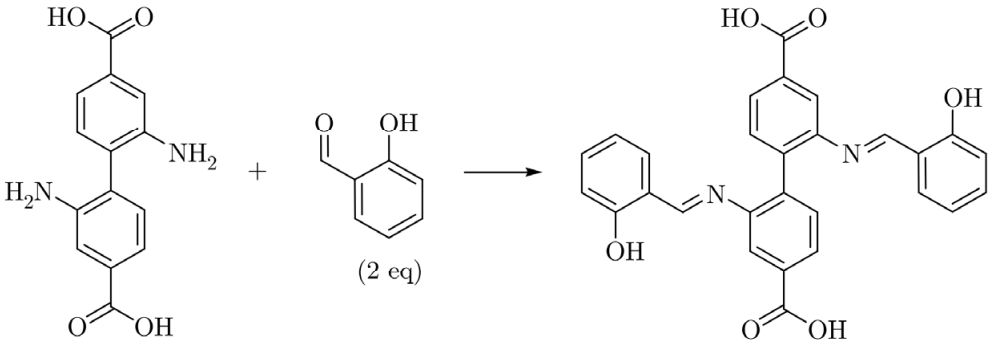


**IV** **$H_4$L**

**Scheme 1.** Synthesis of **$H_4$L**. Reagents and conditions: HCOOH, MeOH, reflux, 20 h.

Synthetic routes to complexes **1** and **2** are shown in Scheme 2. In the reaction of warm methanolic solution of $Cu(CH_3COO)_2 \cdot H_2O$ and warm methanolic solution of $H_4L$, in a 1:1 molar ratio, dark green, block-shaped single crystals of complex $\{[Cu(H_2L)]\cdot x MeOH\}_n$ (**1**) were obtained. By the reaction of $Cu(CH_3COO)_2 \cdot H_2O$ and $H_4L$ in a 1:1 molar ratio, in the presence of HCOOH, at mild solvothermal conditions in DMF at 100 °C for 24 h, brown plate-like single crystals of complex **2** were obtained.

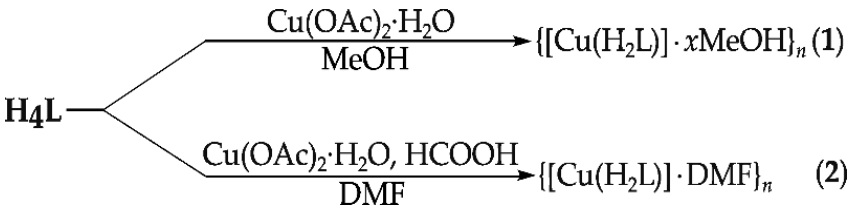


**Scheme 2.** Synthesis and structure of complexes **1** and **2**. Reagents and conditions are shown in the arrows.

Coordination of carboxylic and imine groups of the ligand is confirmed by IR spectroscopy. In the spectra shown in Figure 1, it can be observed that the intensity of vibration band ν(C=O) at 1683 $cm^{-1}$ of the ligand decreases in the case of **1**, which can be explained by the presence of a free carboxylic group in addition to the coordinated carboxylic group. This is in line with results obtained by crystallography (*vide infra*). In addition, there is a shift of this band to 1599 $cm^{-1}$ in **1** and 1660 $cm^{-1}$ in **2**, which indicates the presence of a coordination bond between the copper ion and the carboxylic group. The shift of the ν(C=N) band from 1612 $cm^{-1}$ to lower wavenumbers (1599 $cm^{-1}$ in **1** and 1606 $cm^{-1}$ in **2**) confirms that both nitrogen atoms of the imine groups take a part in forming the coordinate bond.

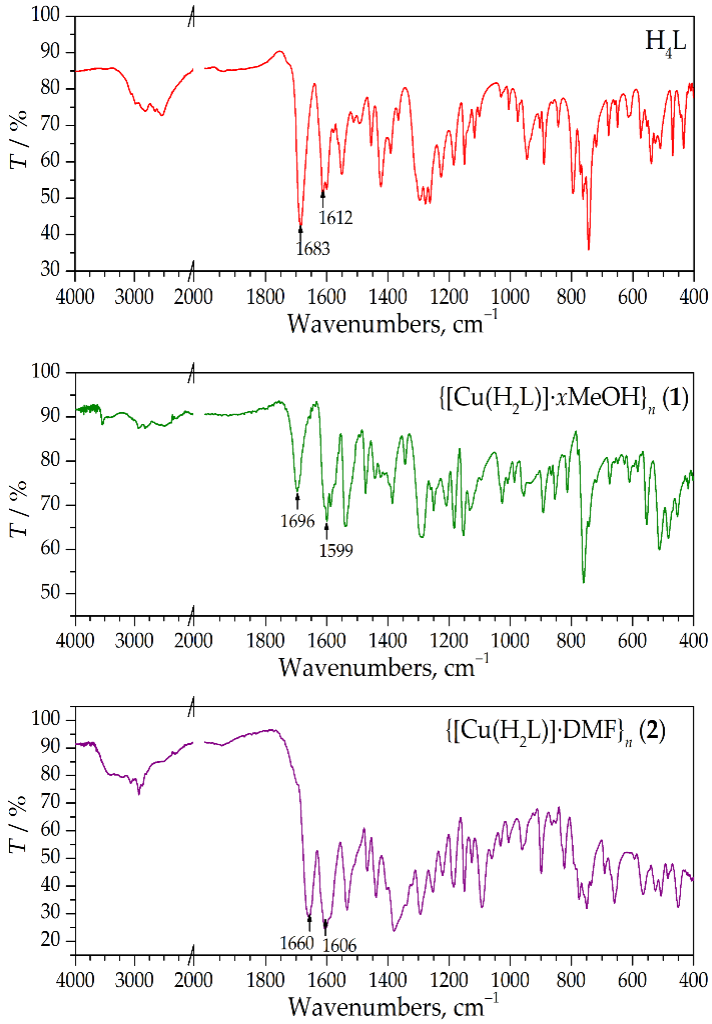


**Figure 1.** IR spectra of the ligand **$H_4$L** and compounds **1** and **2**.

### *2.2. Crystal Structures*

#### 2.2.1. Structure of $H_4L$·3DMF

The crystal structure of ligand **$H_4L$**·3DMF was determined by single-crystal X-ray diffraction. The molecular structure of ligand **$H_4L$** · 3DMF is presented in Figure 2, and selected structural parameters are shown in Table S1 (in the Supplementary Material).

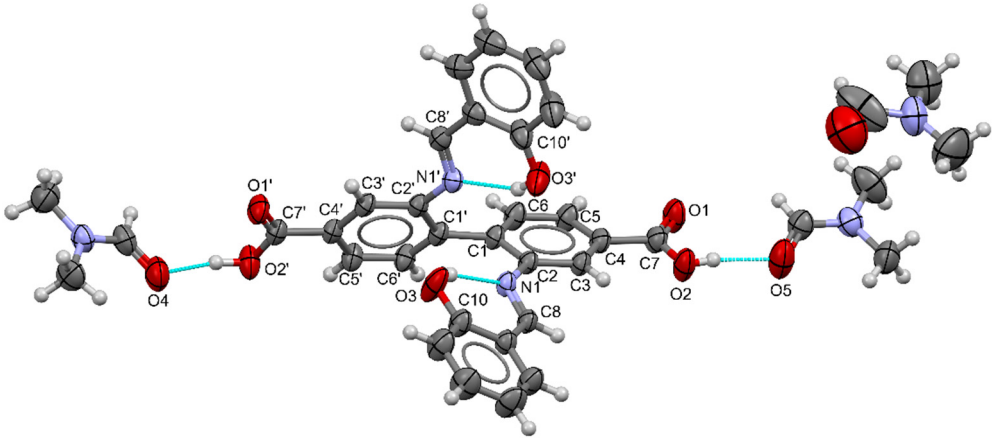


**Figure 2.** The molecular structure of ligand **$H_4L$ · 3DMF** with the numbering of selected atoms. Hydrogen bonds are also shown.

Molecule **$H_4L$** has approximate twofold symmetry, with a pseudo-axis that bisects the C1–C1′ bond. The biphenyl-dicarboxylic core is twisted around the C1–C1′ bond, the dihedral angle between the planes of two phenyl rings is 64.40(6)°, while the torsion angle C2′–C2–C1–C1′ is 66.3(3)°. These torsion angles do not deviate significantly from the corresponding torsion angle found in the structure of 2,2′-diamino-4,4′-biphenyldicarboxylic acid [28], which is 64.2°. This fact indicates that condensation of the rather bulky salicylaldehyde does not have a significant steric influence on the biphenyl-dicarboxylic core conformation.

Both carboxylic groups only slightly deviate from the mean plane through the phenyl cores, which is indicated by the dihedral angles between the planes through the atoms of the phenyl ring C1–C2–C3–C4–C5–C6, i.e., C1′–C2′–C3′–C4′–C5′–C6′ and atoms of the carboxyl group O1–C7–O2–C4, i.e., O1′–C7′–O2′–C4′, which are 6.20(16)° and 5.90(19)°, respectively. The same conclusion is reached if the torsion angles C3–C4–C7–O2 and C5′–C4′–C7′–O2′ are considered, the values of which are 5.7(4)°, and 4.1(3)°, respectively.

The salicylaldehyde fragment is planar and the corresponding dihedral angles between the planes of phenyl rings and salicylaldehyde fragments are 26.00(8)° and 36.80(8)°, respectively. A search of the Cambridge Structural Database (CSD) [29] found 16 compounds containing a 2,2′-bis(((*E*)-2-hydroxybenzylidene)amino)-[1,1′-biphenyl] fragment. The chosen structural parameters of these compounds are summarized in Table S2. Based on the fact that the values of relevant dihedral angles exist in wide intervals: 43.7–89.4° for $\delta$(ph1–ph2), 6.8–41.6° for $\delta$(ph1–sal1), and 10.5–46.7° for $\delta$(ph2–sal2), it can be concluded that these structures have a relatively large degree of conformational freedom. The values of the corresponding angles in the structure of **$H_4L$**·3DMF are similar to the mean values of these ranges.

Selected bond lengths for the ligand are listed in Table 1. The O1-C7, O1′-C7′, N1-C8, and N1′-C8′ bond lengths have the values of a double bond, as expected. By searching the Cambridge Structural Database (CSD) it is found that the structural parameters of **$H_4L$** are in the usual ranges found for compounds with similar structural fragments.

**Table 1.** Selected bond lengths for $H_4L$.

| Bond | Distances (Å) | Bond | Distances (Å) |
|---|---|---|---|
| N1–C8 | 1.273(2) | O1–C7 | 1.217(3) |
| N1′–C8′ | 1.277(3) | O1′–C7′ | 1.201(3) |
| O3–C10 | 1.334(3) | O2–C7 | 1.289(3) |
| O3′–C10′ | 1.344(3) | O2′–C7′ | 1.316(3) |

The asymmetric unit, except for the molecule of **$H_4$L**, consists of three molecules of the solvent DMF. Two intermolecular H–bonds are present between the carboxylic groups of **$H_4$L** and O atoms of the carbonyl group in two molecules of DMF, while the third molecule of DMF does not participate in hydrogen bonding. Additionally, two intramolecular O–H···N hydrogen bonds are present in **$H_4$L**, both between the imine and hydroxyl groups of the salicylaldehyde fragment. Table 2 lists details of the H-bond parameters.

**Table 2.** Hydrogen bonding geometry parameters for $H_4L$.

| Bond | Distances (Å) | | | Angles (°) |
|---|---|---|---|---|
| *D*–H···*A* | *D*–H | H···*A* | *D*···*A* | *D*–H···*A* |
| O2–H2···O5 | 0.82 | 1.76 | 2.574(3) | 170.4 |
| O2′–H2′···O4 | 0.82 | 1.78 | 2.596(2) | 177.8 |
| O3–H3O···N1 | 0.90(4) | 1.78(4) | 2.611(2) | 154(3) |
| O3′–H3O′···N1′ | 0.92(3) | 1.74(3) | 2.611(2) | 158(3) |

### 2.2.2. Crystal Structures of Complexes

Complexes $\{[Cu(H_2L)]\cdot x\text{MeOH}\}_n$ (**1**) and $\{[Cu(H_2L)]\cdot\text{DMF}\}_n$ (**2**) are solvatomorphs, and their crystal structures consist of the packing of monoperiodic polymeric molecules $\{[Cu(H_2L)]\}_n$, with solvent molecules filling the voids. The molecular structures of the monomeric units and atom numbering schemes are presented in Figure 3.

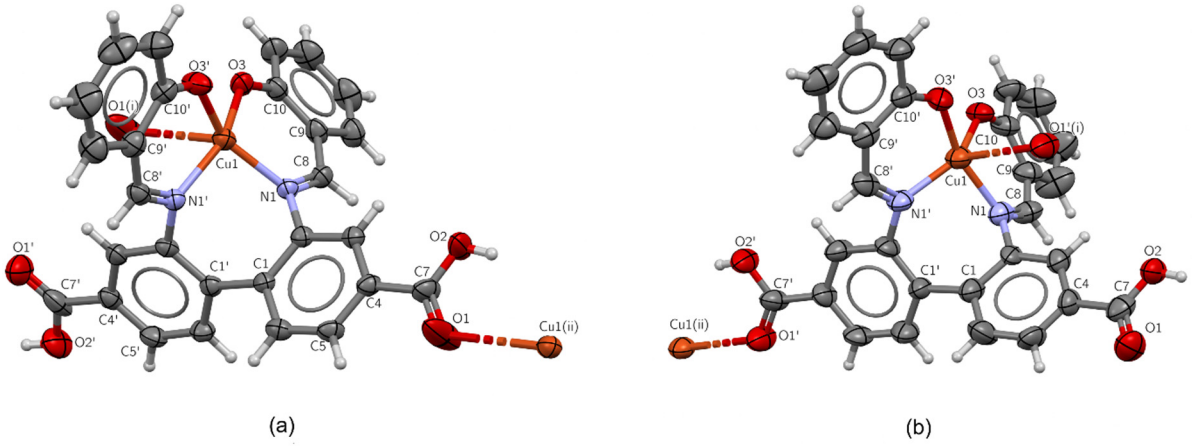


**Figure 3.** Molecular structures of monomeric units with the atom numbering scheme. (**a**) $\{[Cu(H_2L)]\cdot x\text{MeOH}\}_n$ (**1**); (**b**) $\{[Cu(H_2L)]\cdot\text{DMF}\}_n$ (**2**). DMF molecules in **2** are omitted for the sake of clarity.

In both complexes, the ligand exists as a dianion ($H_2L^{2-}$) formed by the deprotonation of both phenolic oxygen atoms. The ligand is coordinated in a pentadentate manner, through both phenoxide oxygen atoms and both azomethine nitrogen atoms, while the oxygen atom of one carboxylate has a bridging role, binding the copper atom of the neighboring unit. The polydentate nature of the ligand coordination results in the formation of three fused metallocycles, two six-membered (almost flat) and one seven-membered, which is significantly puckered.

Polymeric chains propagate along crystallographic axis *a* for **1** and axis *b* for **2**, with translation as the repeating symmetry operation. The closest Cu···Cu distance within the chain is 9.812(2) Å for **1** and 9.8628(9) Å for **2**. Structures of the monomeric units have approximate twofold rotational symmetry with the pseudo-axis incorporating the Cu1 atom and bisecting the C1—C1′ bond. In complex **2**, conformations of carboxylic groups break this pseudosymmetry, as they are in opposite orientations with respect to the phenyl rings, as reflected through the torsion angles $\tau$(O1–C7–C4–C5) = 3.9(9)° and $\tau$(O1′–C7′–C4′–C5′) = 179.0(5)°.

In both complexes, the coordination number of Cu(II) is five. The shortest bonds within the coordination polyhedron involve deprotonated phenoxide oxygen atoms (*d*(Cu–O) in the range of 1.899(4)–1.924(5) Å), while slightly longer are the bonds involving azomethine nitrogen atoms (*d*(Cu–N) in the range of 1.941(6)–1.995(6) Å), as presented in Table 3. These values are in line with those found for Cu(II) complexes with structurally similar ligands [30–38]. The oxygen atom of one carboxylate group participates in a bond of a significantly longer length compared to the rest of the metal–ligand bonds (2.626(5) Å in **1** and 2.774(4) Å for **2**).

**Table 3.** Selected bond lengths for complexes **1** and **2**.

| Bond | Distances (Å) | |
|---|---|---|
| | **1** | **2** |
| Cu1–O3 | 1.924(5) | 1.912(3) |
| Cu1–O3′ | 1.902(5) | 1.899(4) |
| Cu1–N1 | 1.941(6) | 1.976(4) |
| Cu1–N1′ | 1.995(6) | 1.954(4) |
| Cu1–O1′(*i*) | 2.626(5) | 2.774(4) |

It is quite challenging to assign a coordination polyhedron to the Cu(II) coordination environment of complexes **1** and **2**. Addison's trigonality indices ($\tau_5$ = 0.24 for **1** and $\tau_5$ = 0.09 for **2**) assign polyhedrons to deformed square pyramids (*SPY*-5) [39]. Conversely, Holmes' dihedral angle method [40,41] results in the opposite assignment—polyhedra traversed 23% (for **1**) and 34% (for **2**) along $D_{3h} \rightarrow C_{4v}$ Berry pseudorotational pathway—which classifies them as deformed trigonal bipyramids (*TBPY*-5). Calculations of continuous shape measures [42] add strength to the Holmes' method assignment, as results show that the polyhedra are closer to trigonal bipyramid (*S*(*TBPY*-5) = 2.067 for **1** and *S*(*TBPY*-5) = 2.984 for **2**) than to square pyramid (*S*(*SPY*-5) = 5.038 for **1** and *S*(*SPY*-5) = 4.505 for **2**). Still, their shapes significantly deviate from the minimum distortion interconversion path, indicating that deformation does not follow the Berry pseudorotation pathway.

Though individual polymeric molecules of complexes **1** and **2** have the same structural formula $\{[Cu(H_2L)]\}_n$, their packing in the crystal structure is significantly different (as can be seen in Figure 4). In both complexes, the coordinated carboxylic group is hydrogen-bonded to a deprotonated phenoxide oxygen of the neighboring monomeric unit within the chain. An uncoordinated carboxylic group connects neighboring polymeric chains by the formation of an intermolecular hydrogen bond with deprotonated phenoxide oxygen in **1**, thus forming sheets parallel to the *ab* plane. In **2**, the uncoordinated carboxylic group is hydrogen-bonded to the DMF molecule, as depicted in Figure 4. It may be speculated that MeOH molecules are disordered within the crystal structure of **1** due to a lack of ability to form strong hydrogen bonds, as all potential H-bond donors are already saturated. The structural parameters of the hydrogen bonding in **1** and **2** are listed in Table S3 in the Supplementary Material.

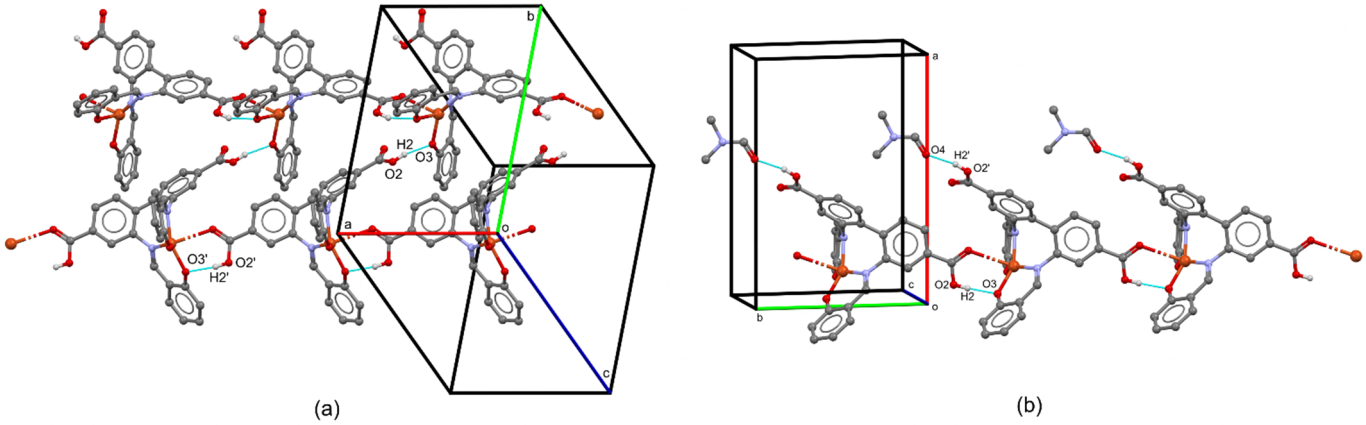


**Figure 4.** Hydrogen bonding in the complexes. (**a**) {[Cu($H_2$L)]·*x*MeOH}$_n$ (**1**); (**b**) {[Cu($H_2$L)]·DMF}$_n$ (**2**).

It is interesting to note that the phenyl rings of the salicylidene residues are stacked with weak π–π interactions, and are involved in CH–π interactions that further connect the hydrogen-bonded polymeric sheets of **1** and polymeric chains of **2**, as depicted in Figures S7 and S8. Details of these interactions are given in Table S4.

### *2.3. Thermal Properties of the Ligand and Complexes*

The ligand, 2,2′-bis(((*E*)-2-hydroxybenzylidene)amino)-[1,1′-biphenyl]-4,4′-dicarboxylic acid (**$H_4$L**), and its coordination compounds with Cu(II) were characterized by thermoanalytical measurements in argon. **$H_4$L** begins to decompose at 72 °C, *onset*, in two well-defined steps (Figure 5). In the first step, with a DTG maximum at 91 °C, **$H_4$L** loses 7.8% of its mass, which is less than the evaporation of one DMF molecule (10.46%). In the next step, the mass decreases by an additional 21.0% at a relatively low temperature with a DTG maximum of 119 °C. The low-temperature range and the mass losses suggest the spontaneous evaporation of lattice DMF (31.38% of the mass) during storage. The mechanism of the desolvation is in accordance with the crystal structure of the ligand. Namely, one of the three lattice DMF molecules is bonded somewhat more weakly to the ligand molecules, while the other two DMF molecules are bonded with stronger interactions. The DMF molecule stabilized by weaker interactions evaporates at a lower temperature, while the other two stronger bonded molecules evaporate at a ~30 °C higher temperature. The desolvation finishes up to 250 °C, and the desolvated ligand is formed. It is stable up to 301 °C, *onset*. Above this temperature, **$H_4$L** decomposes but the decomposition is not finished up to 500 °C and a carbonaceous final residue is isolated.

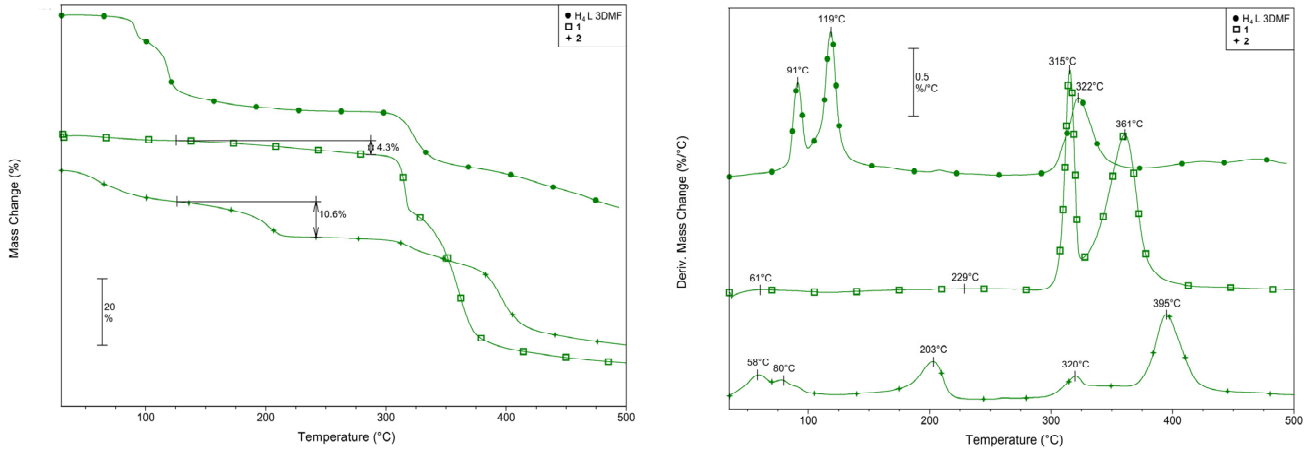


**Figure 5.** TG (**left**) and DTG (**right**) curves of the $H_4$L, **1** and **2** recorded in argon.

On the DSC curve of the ligand, the endothermic peaks of solvent evaporation at 94 and 121 °C are detected. The thermal decomposition of the ligand is also followed by an endothermic heat effect with a peak at 312 °C.

The thermal decomposition of the complex polymer {[Cu($H_2$L)]·$x$MeOH}$_n$ (**1**) begins at room temperature with a loss of 1.3% of its mass up to ~125 °C (Figure 5). This mass loss step most probably corresponds to lattice methanol loss. Due to interactions between the lattice solvent and the complex polymer chain, the evaporation of the solvent molecules is slow and persists across a relatively large temperature range. By X-ray diffraction, about 1−2 molecules of MeOH were found, but these methanol molecules are disordered and their exact number cannot be determined in this way. Without reference to the exact number of lattice MeOHs, the approximate mass percent of this fraction was calculated. To estimate the minimal methanol content of **1**, for approximation, one MeOH molecule per monomeric unit of **1** was used. In accordance, the mass loss in this first step (1.3%) is significantly less than the calculated mass percent of methanol (5.6%) calculated for one molecule of MeOH per monomeric unit. Despite the approximation of the methanol content of **1**, such a big difference between the calculated and measured values suggests spontaneous evaporation of methanol during storage. Above ~150 °C a slower mass loss process of low intensity begins and, up to 287 °C, the mass of **1** decreases by 4.3%. Considering the high-temperature range of this process, this is most probably the beginning of the thermal degradation of **1**. Above 299 °C, onset occurs in two more intensive steps with mass losses of 17.9 and 45.5%. The corresponding DTG maxima are at 315 and 361 °C. Comparison of the TA curves of **1** with the TA curves of the ligand suggests that the process with a DTG maximum at 315 °C corresponds to the main processes of thermal degradation of the ligand. The differences between the decomposition mechanism of the ligand and complex **1** are the result of their different structures. Above 400 °C the decomposition process slows down and does not finish up to 700 °C.

The DSC analysis shows that all steps of the thermal decomposition of **1** are endothermic.

The thermal decomposition of complex polymer {[Cu($H_2$L)]·DMF}$_n$ (**2**) also begins with desolvation from room temperature, in a manner similar to **1**. In the first two overlapped steps, **2** loses 6.0 and 4.8% of its mass, respectively. This total of 10.8% may correspond to DMF evaporation from the sample. The DMF content calculated for one monomeric unit of the complex polymer is 11.88%. The corresponding DTG peaks appear at 58 and 79 °C (Figure 5). Above 100 °C, the mass loss rate slows down up to ~170 °C; above this temperature, **2** loses 10.6% of its mass. A DTG maximum is detected at 202 °C. The next significant mass loss occurs above 300 °C. The detected mass changes are 5.9 and 24.2%, respectively, and the corresponding DTG maxima are at 320 and 395 °C, respectively. Due to the polymeric nature of the compound, it is hard to predict the evolved fragments in these steps without coupled measurements.

The DSC curve of **2** is somewhat different from that of the previous compound. This shows that the decomposition processes are followed by an endothermic heat effect up to ~330 °C, while above this temperature the degradation became slightly exothermic.

To prove the evaporation of the solvents, coupled TG–MS measurements were carried out. The analysis of the ligand showed that, in the first two mass loss steps with DTG maxima at 91 and 119 °C, besides DMF (15, 18, 29, 30, 44 $m/z$) there is also absorbed moisture (17, 18 $m/z$) (Figure 6). This suggests that DMF evaporates spontaneously during storage and, in place of the lost DMF, the ligand absorbs moisture from the atmosphere. During the next mass loss with a DTG maximum at 322 °C, fragments with $m/z$ = 17, 18, 29, and 44 are detected due to the degradation of the ligand and formation of $H_2O^+$, $CHO^+$, and $CO_2{}^+$.

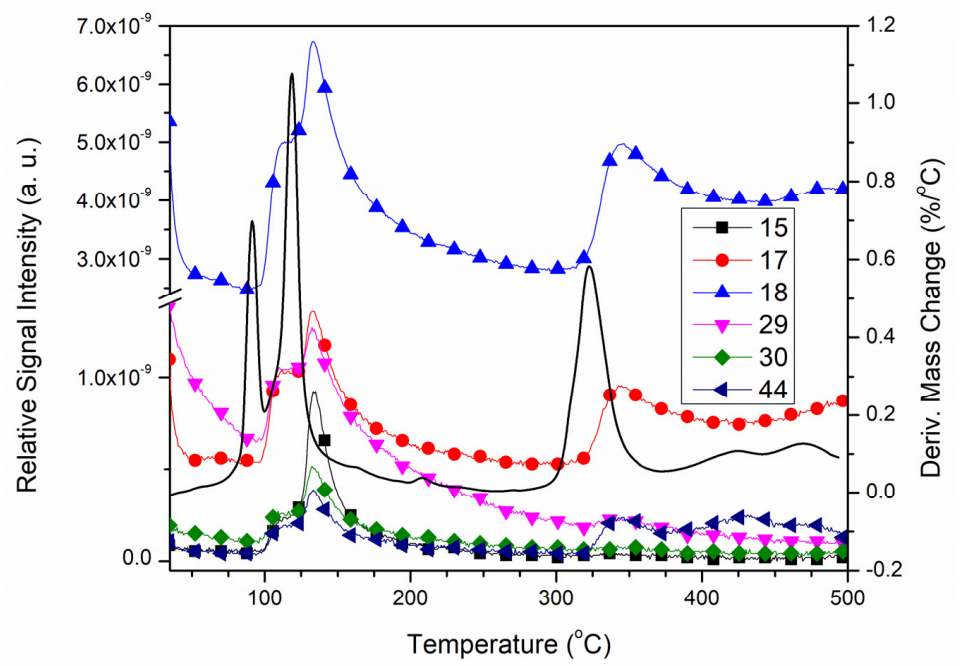


**Figure 6.** TG–MS signals of fragments evolved from **$H_4$L** during heating in argon.

The freshly prepared coordination polymer **1** contains lattice methanol, but it is not detected by TG–MS. The low mass loss up to ~125 °C suggests the spontaneous evaporation of lattice methanol. Instead of methanol, water evaporates from the sample of **1** in the first mass loss step with a DTG maximum at 61 °C (Figure 7). This suggests that, besides the evaporation of the lattice methanol, **1** absorbed some water during storage. The mass decrease of 1.3% shows that the amount of absorbed water is significantly less than the methanol content of the freshly prepared compound **1** (5.6% approximately for **1·MeOH**), and it is most probably only superficially bonded water.

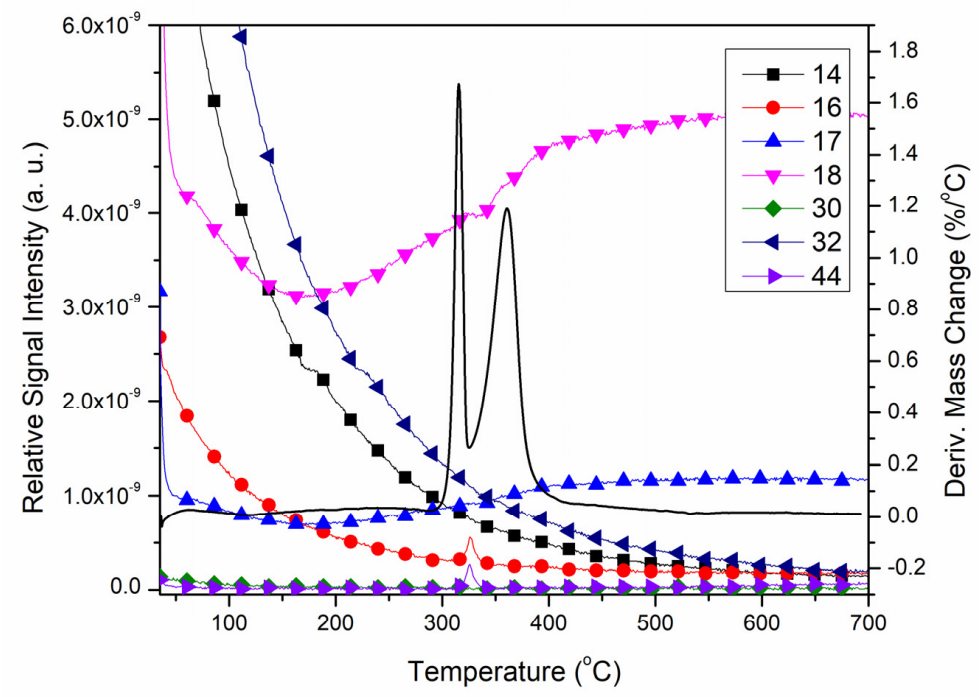


**Figure 7.** TG–MS signals of fragments evolved from **1** during heating in argon.

Due to the very low intensity and wide temperature range of the mass change in the next step (~150–290 °C), it is hard to detect the evolved fragments because of their low amount. The increase in the intensity of the signals 17 and 18 $m/z$ suggests that, besides $m/z$ = 14 and 32, fragments of $OH^+$ and $H_2O^+$ also form. However, at such high temperatures, the water is most probably a degradation product of the compound. The most intensive degradation steps above 300 °C are followed by the evolution of fragments $m/z$ = 16 ($O^+$ or $NH_2^+$), 17, 18 ($OH^+$ and $H_2O^+$), and 44 ($CO_2^+$). The detected fragments are in accordance with the composition and structure of the compound.

A fresh sample of **2** contains one molecule DMF per monomeric unit of the coordination polymer. However, the results of TG–MS analysis also proved the spontaneous evaporation of DMF from this sample, in common with the ligand. Fragments, characteristic for DMF: $CH_3^+$, $CHO^+$ and/or $CH_3N^+$, and $NC_2H_6^+$ (15, 29, and 44 $m/z$), give peaks of low intensity, unlike the fragments of water (17 and 18 $m/z$ in intensity ratio 1:4) (Figure 8). The water content separate from DMF was demonstrated by recording IR spectra (Figure S2). In the spectrum of **2**, recorded by the ATR technique, the characteristic wide band of water appears at 3393 $cm^{-1}$. Despite this, in the spectrum of the desolvated form of **2** isolated as an intermediate after complete desolvation at 130 °C by stepwise isothermal technique, this band is missing. One more band is significantly changed in the IR spectrum of desolvated **2**: the intensive band at 1663 $cm^{-1}$ is significantly less intensive than that in the spectrum of **2**. However, as the IR bands of DMF and the ligand are principally overlapped, the intensity decrease in some bands is most probably a result of the evaporation of DMF, especially at low temperatures. In the mass-loss steps above 170 °C, evaporation fragments of the ligand and, in addition to water and $CO_2$, fragments 14, 16, 29, 30, and 36 $m/z$ were also detected. They originate from the degradation of the coordinated ligand.

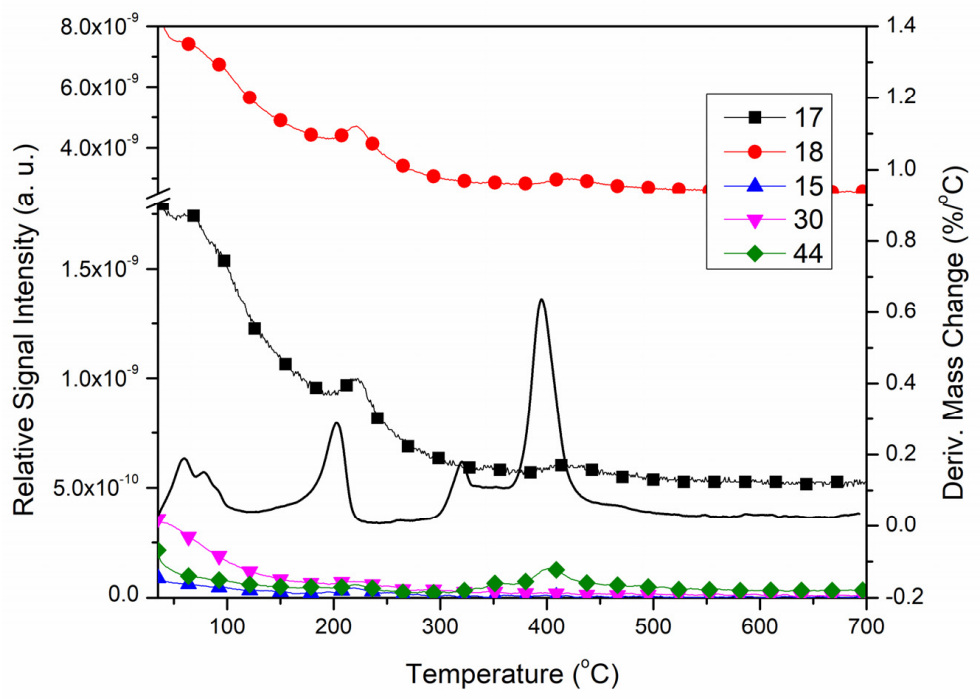


**Figure 8.** TG–MS signals of fragments evolved from **2** during heating in argon.

The spontaneous evaporation of lattice DMF and absorption of water into the free vacancies in the crystal lattice may be explained by the different polarities of these solvents. DMF is less polar than water and the $H_2O$ molecule is less voluminous than DMF. Thus, because of fewer and weaker interactions with the main compound in the crystal lattice, DMF can easily evaporate. Conversely, $H_2O$ easily forms numerous interactions with the molecules in the crystal lattice due to its polarity.

## 3. Materials and Methods

### *3.1. Materials and Physical Measurements*

Chemical reagents as well as solvents were used as supplied without further purification. IR spectra were recorded on a Thermo Nicolet iS20 FTIR spectrophotometer (Thermo Fisher SCIENTIFIC) with Smart iTR™ ATR Sampling accessories, in a range of 4000–400 $cm^{-1}$. $^{1}H$ and $^{13}C$ NMR spectra were recorded with a Bruker AVANCE III 400 spectrometer operating at 400 MHz for $^{1}H$ NMR and 100 MHz for $^{13}C$ NMR. Residual solvent signals were used for the chemical shift (ppm; δ-scale) calibration. Two-dimensional experiments (gradient $^{1}H$–$^{1}H$ COSY, HSQC, and HMBC; and NOESY) and DEPT-135 were run utilizing built-in Bruker pulse sequences.

The simultaneous thermogravimetric–differential scanning calorimetric measurements (TG–DSC) were carried out on a TA Instruments SDT Q600 thermal analyzer from room temperature up to 700 °C in the atmosphere of argon and flow rate 50 $cm^3$ $min^{-1}$. The heating rate was 10 °C $min^{-1}$. The sample (1–2 mg) was placed in an alumina crucible, and an empty alumina crucible was the reference. The analysis of the evolved gaseous products was carried out on a Hiden Analytical HPR20/QIC mass spectrometer coupled to the SDT Q600 thermal analyzer. The selected fragments from 15 to 80 $m/z$ mass values were followed in Multiple Ion Detection (MID) modes.

### *3.2. Preparation of the Compounds*

#### 3.2.1. **$H_4L$**

2,2′-diamino-[1,1′-biphenyl]-4,4′-dicarboxylic acid (272.3 mg, 1 mmol) and salicylaldehyde (0.2 mL, 2 mmol) were mixed in a 1:2 molar ratio in methanol (10 mL), followed by the addition of formic acid (1 mL). The solution was stirred and heated to reflux for 20 h, after which a yellow precipitate formed. The precipitate was collected, washed with cold methanol, and dried in a vacuum. Yield: 397 mg, 82%. $^{1}H$ NMR (400 MHz, DMSO-$d_6$, ppm): 13.29 (br s, 2H, COOH), 12.23 (s, 2H, Ar-OH), 8.92 (s, 2H, H8), 8.08 (s, 2H, H3), 7.98 (d, $J$ = 7.9 Hz, 2H, H5), 7.54 (d, $J$ = 7.9 Hz, 2H, H6), 7.47 (d, $J$ = 7.7 Hz, 2H, H14), 7.33 (dd, $J$ = 8.4, 7.4 Hz, 2H, H12), 6.86 (dd, $J$ = 7.7, 7.4 Hz, 2H, H13), 6.78 (d, $J$ = 8.4 Hz, 2H, H11). $^{13}C$ NMR (101 MHz, DMSO-$d_6$, ppm): 167.36 (C7), 164.83 (C8), 160.48 (C10), 146.92 (C2), 139.01 (C1), 133.98 (C12), 133.35 (C14), 132.54 (C4), 131.24 (C6), 128.04 (C5), 119.56 (C9), 119.53 (C13), 119.34 (C3), 116.87 (C11). $\nu_{max}/cm^{-1}$ (ATR): 2582 w, 2542 w, 1936 w, **1683** s, **1612** s, 1600 s, 1550 m, 1512 w, 1494 w, 1455 m, 1423 s, 1391 m, 1366 w, 1296 s, 1277 s, 1263 s, 1226 m, 1185 m, 1150 m, 1117 m, 1101 w, 1031 w, 1005 w, 976 w, 946 m, 904 w, 890 m, 844 w, 795 s, 772 m, 762 s, 744 s, 720 m, 679 m, 659 w, 650 w, 615 w, 574 m, 554 w, 540 m, 526 m, 510 m, 470 m, 434 m, 411 w.

After recrystallization from DMF, yellow single crystals of **$H_4L$** dimethylformamide threesolvate (**$H_4L$**·3DMF) suitable for structural analysis were obtained.

#### 3.2.2. {[Cu($H_2L$)]·x$MeOH$}$_n$ (1)

To a warm solution of $H_4L$ (48.1 mg, 0.1 mmol) in MeOH (8 mL), a warm solution of $Cu(CH_3COO)_2 \cdot H_2O$ (20.8 mg, 0.1 mmol) in MeOH (2 mL) was added. The solution was then left to evaporate to a small volume at room temperature. Green plate-like single crystals were isolated by filtration, washed with MeOH, and air-dried overnight. Yield: 12 mg (21%). $\nu_{max}/cm^{-1}$ (ATR): 3546 w, 2933 w, 2824 w, 2496 w, 2347 w, 1923 w, **1696** w, **1599** s, 1587 m, 1540 s, 1473 m, 1442 w, 1424 w, 1385 m, 1344 w, 1287 s, 1250 m, 1209 m, 1183 s, 1152 s, 1132 m, 1027 m, 1008 w, 987 w, 955 m, 892 m, 866 w, 854 m, 813 w, 779 w, 760 s, 743 s, 675 w, 649 w, 626 w, 610 w, 583 w, 554 s, 512 s, 483 s, 453 m, 423 w, 418 w, 403 w.

#### 3.2.3. {[Cu($H_2L$)]·$DMF$}$_n$ (2)

$Cu(OAc)_2 \cdot H_2O$ (16.1 mg, 0.08 mmol) was dissolved in DMF (1 mL) at room temperature. To this solution, a solution of $H_4L$ (38.7 mg, 0.08 mmol) in DMF (2 mL) was added. The glass vial was placed in a thermoblock at 100 °C for 48 h and then cooled to room temperature. The brown block-shaped single crystals suitable for X-ray diffraction of **2**

were obtained. Yield: 2.9 mg, 6%. $\nu_{max}/cm^{-1}$ (ATR): 3065 w, 2927 w, 1943 w, **1660** s, **1606** s, 1533 s, 1467 w, 1439 m, 1380 s, 1294 s, 1253 m, 1221 m, 1184 m, 1150 m, 1126 w, 1092 s, 1060 w, 1032 w, 1005 w, 961 w, 899 w, 864 w, 823 w, 775 m, 749 s, 691 w, 659 m, 594 w, 565 m, 525 m, 507 m, 485 m, 452 s.

### *3.3. Crystal Structure Determination*

X-ray diffraction experiments were performed on a four-circle single crystal X-ray diffractometer Gemini S (Oxford Diffraction), equipped with a position-sensitive CCD detector Sapphire3. Measurements were made at room temperature. Iterative dual-space routines implemented in *SHELXT* [43] were used to solve crystal structures, which were subsequently refined with *SHELXL* [44]. All non-hydrogen atoms were refined anisotropically. Hydrogen atoms were placed in idealized positions and refined using a riding model.

The crystal structure of **1** contains voids filled with heavily disordered methanol molecules. As all attempts to model disorder were unsuccessful, the *PLATON* SQUEEZE [45] procedure was employed to obtain reasonable refinement statistics. Four symmetry-related voids are present in the unit cell (one per monomeric unit of the complex). A void has a volume of 140 $Å^3$ and its content was determined to be 30 electrons. This corresponds to roughly 1.5 molecules of MeOH. Having in mind the approximate nature of the SQUEEZE procedure, it is plausible that *x* in the formula of **1** can take any value from 1 to 2.

Crystal structures were validated internally with *PLATON* [46] and externally with the Cambridge Structural Database (CSD) [29] through *MOGUL* knowledge bases [47] accessible through *Mercury CSD* [48]. Pertinent crystallographic and refinement details are given in Table S1.

CCDC 2218514-2218516 contains the supplementary crystallographic data for this paper. These data can be obtained free of charge from The Cambridge Crystallographic Data Centre via www.ccdc.cam.ac.uk/structures.

## 4. Conclusions

Condensation of salicylaldehyde with 2,2′-diamino-[1,1′-biphenyl]-4,4′-dicarboxylic acid gave a new Schiff base ligand, as a representative of a rare class of Schiff bases where the azomethine functional group is coupled to biphenyl rings of an [1,1′-biphenyl]-dicarboxylic acid.

This polyfunctional ligand, containing carboxylic, imino, and phenol functional groups, was shown to be able to form monoperiodic polymeric complexes with copper(II). These polymorphs crystallize with solvent molecules and are shown to be able partially exchangeable with water.

The bridging coordination mode of the ligand was achieved through one carboxylic group, leaving the second one free to form hydrogen bonds. In perspective, it appears viable to search for reaction conditions in which both carboxylic groups may be involved in coordination, possibly in a bridging mode, therefore potentially leading to polymers of periodicity higher than one. Such polymers may show higher porosity and, therefore, could have a higher potential for application in adsorption or catalysis.

**Supplementary Materials:** The following supporting information can be downloaded at: https://www.mdpi.com/article/10.3390/inorganics10120261/s1, Figure S1. FTIR spectrum of **IV**; Figure S2. FTIR spectra of 2 and its desolvated form; Figure S3. $^1$H NMR spectra (400 MHz, DMSO-$d_6$) of **IV**; Figure S4. $^1$H NMR spectra (400 MHz, DMSO-$d_6$) of $\mathbf{H_4L}$; Figure S5. $^{13}$C NMR (101 MHz, DMSO-$d_6$) of $\mathbf{H_4L}$; Figure S6. Relevant HMBC (in gray), COSY (in red), and NOESY (in blue) correlations of $\mathbf{H_4L}$; Table S1. Crystallographic and refinement details; Table S2. Selected dihedral angles of structures with the bis(salicylaldehyde)-2,2′-diaminobiphenyl fragment; Table S3. Hydrogen-bonding geometry parameters for complexes 1 and 2; Table S4. Structural parameters of π···π and C–H···π interactions in the crystal structures of 1 and 2; Figure S7. Intermolecular π···π and C–H···π interactions in the crystal structure of 1. Only relevant hydrogen atoms involved are shown; Figure S8. Intermolecular π···π and C–H···π interactions in the crystal structure of 2. Only relevant hydrogen atoms involved are shown.

**Author Contributions:** Conceptualization, M.G.B., M.V.R. and B.B.H.; investigation, M.G.B., N.D.R., M.V.R., V.N.R., B.B.K. and B.B.H.; resources, B.B.H.; writing—original draft preparation, M.G.B., M.V.R., B.B.H., M.M.R. and N.D.R.; writing—review and editing, B.B.H., M.V.R. and M.M.R.; visualization, M.G.B. and B.B.H.; supervision, L.S.V.-J., M.V.R. and M.M.R.; project administration, M.V.R. and M.M.R.; funding acquisition, B.B.H., M.V.R. and M.M.R. All authors have read and agreed to the published version of the manuscript.

**Funding:** This research was funded by the Science Fund of the Republic of Serbia, PROMIS grant number 6066708 (CASCH-MOF), the Ministry of Education, Science and Technological Development of the Republic of Serbia (Grant No. 451-03-68/2022-14/200125), and the Provincial Secretariat for Higher Education and Scientific Research (Grant No. 142-451-2197/2022).

**Data Availability Statement:** Not applicable.

**Conflicts of Interest:** The authors declare no conflict of interest.

## References

1. Tombesi, A.; Pettinari, C. Metal Organic Frameworks as Heterogeneous Catalysts in Olefin Epoxidation and Carbon Dioxide Cycloaddition. *Inorganics* **2021**, *9*, 81. [CrossRef]
2. Ristić, P.; Filipović, N.; Blagojević, V.; Ćirković, J.; Barta Holló, B.; Đokić, V.R.; Donnard, M.; Gulea, M.; Marjanović, I.; Klisurić, O.R.; et al. 2D and 3D Silver-Based Coordination Polymers with Thiomorpholine-4-Carbonitrile and Piperazine-1,4-Dicarbonitrile: Structure, Intermolecular Interactions, Photocatalysis, and Thermal Behavior. *CrystEngComm* **2021**, *23*, 4799–4815. [CrossRef]
3. Ristić, P.; Todorović, T.R.; Blagojević, V.; Klisurić, O.R.; Marjanović, I.; Barta Holló, B.; Vulić, P.; Gulea, M.; Donnard, M.; Monge, M.; et al. 1D and 2D Silver-Based Coordination Polymers with Thiomorpholine-4-Carbonitrile and Aromatic Polyoxoacids as Coligands: Structure, Photocatalysis, Photoluminescence, and TD-DFT Study. *Cryst. Growth Des.* **2020**, *20*, 4461–4478. [CrossRef]
4. Brezovan, M.; Juráková, J.; Moncol, J.; Dlháň, Ľ.; Korabik, M.; Šalitroš, I.; Pavlik, J.; Segľa, P. The Role of the Bridge in Single-Ion Magnet Behaviour: Reinvestigation of Cobalt(II) Succinate and Fumarate Coordination Polymers with Nicotinamide. *Inorganics* **2022**, *10*, 128. [CrossRef]
5. Bazhenova, T.A.; Mironov, V.S.; Yakushev, I.A.; Svetogorov, R.D.; Maximova, O.v; Manakin, Y.v; Kornev, A.B.; Vasiliev, A.N.; Yagubskii, E.B. End-to-End Azido-Bridged Lanthanide Chain Complexes (Dy, Er, Gd, and Y) with a Pentadentate Schiff-Base [$N_3O_2$] Ligand: Synthesis, Structure, and Magnetism. *Inorg. Chem.* **2020**, *59*, 563–578. [CrossRef]
6. Khattak, Z.A.K.; Ahmad, N.; Younus, H.A.; Ullah, H.; Yu, B.; Munawar, K.S.; Ashfaq, M.; Ali, S.; Shahadat, H.M.; Verpoort, F. Synthesis of 3D Cadmium(II)-Carboxylate Framework Having Potential for Co-Catalyst Free $CO_2$ Fixation to Cyclic Carbonates. *Inorganics* **2022**, *10*, 162. [CrossRef]
7. Demakov, P.A.; Volynkin, S.S.; Samsonenko, D.G.; Fedin, V.P.; Dybtsev, D.N. A Selenophene-Incorporated Metal–Organic Framework for Enhanced $CO_2$ Uptake and Adsorption Selectivity. *Molecules* **2020**, *25*, 4396. [CrossRef]
8. Kravtsov, V.C.; Lozovan, V.; Siminel, N.; Coropceanu, E.B.; Kulikova, O.v.; Costriucova, N.v.; Fonari, M.S. From 1d to 2d Cd(Ii) and Zn(Ii) Coordination Networks by Replacing Monocarboxylate with Dicarboxylates in Partnership with Azine Ligands: Synthesis, Crystal Structures, Inclusion, and Emission Properties. *Molecules* **2020**, *25*, 5616. [CrossRef]
9. Troyano, J.; Zapata, E.; Perles, J.; Amo-Ochoa, P.; Fernández-Moreira, V.; Martínez, J.I.; Zamora, F.; Delgado, S. Multifunctional Copper(I) Coordination Polymers with Aromatic Mono- and Ditopic Thioamides. *Inorg. Chem.* **2019**, *58*, 3290–3301. [CrossRef]
10. Michaels, H.; Golomb, M.J.; Kim, B.J.; Edvinsson, T.; Cucinotta, F.; Waddell, P.G.; Probert, M.R.; Konezny, S.J.; Boschloo, G.; Walsh, A.; et al. Copper Coordination Polymers with Selective Hole Conductivity. *J. Mater. Chem. A Mater.* **2022**, *10*, 9582–9591. [CrossRef]
11. Dzhardimalieva, G.I.; Baimuratova, R.K.; Knerelman, E.I.; Davydova, G.I.; Kudaibergenov, S.E.; Kharissova, O.v.; Zhinzhilo, V.A.; Uflyand, I.E. Synthesis of Copper(II) Trimesinate Coordination Polymer and Its Use as a Sorbent for Organic Dyes and a Precursor for Nanostructured Material. *Polymers* **2020**, *12*, 1024. [CrossRef] [PubMed]
12. Liu, X.; Hamon, J.R. Recent Developments in Penta-, Hexa- and Heptadentate Schiff Base Ligands and Their Metal Complexes. *Coord. Chem. Rev.* **2019**, *389*, 94–118. [CrossRef]
13. Kaczmarek, M.T.; Zabiszak, M.; Nowak, M.; Jastrzab, R. Lanthanides: Schiff Base Complexes, Applications in Cancer Diagnosis, Therapy, and Antibacterial Activity. *Coord. Chem. Rev.* **2018**, *370*, 42–54. [CrossRef]
14. Radanović, M.M.; Barta Holló, B. Some Aromatic Schiff Bases and Their Metal Complexes. In *Schiff Base in Organic, Inorganic and Physical Chemistry*; IntechOpen Limited: London, UK, 2022; pp. 1–32.
15. Segura, J.L.; Mancheño, M.J.; Zamora, F. Covalent Organic Frameworks Based on Schiff-Base Chemistry: Synthesis, Properties and Potential Applications. *Chem. Soc. Rev.* **2016**, *45*, 5635. [CrossRef]
16. Clarke, R.M.; Storr, T. The Chemistry and Applications of Multimetallic Salen Complexes. *Dalton Trans.* **2014**, *43*, 9380. [CrossRef]
17. Kudyakova, Y.S.; Bazhin, D.N.; Goryaeva, M.v; Burgart, Y.v; Saloutin, V.I. The Use of 2-(1-Alkoxyalkylidene)-1,3-Dicarbonyl Compounds in Organic Synthesis. *Russ. Chem. Rev.* **2014**, *83*, 120–142. [CrossRef]

18. Dammert, W. Disazomethin-Pigmentfarbstoff Federal Republic of Germany Patent. DE1963403 A, 15 July 1971.
19. Suthar, B.P.; Patel, S.R. Synthesis and Characterization of Poly Schiff Bases from Benzidine-3,3′-Dicarboxylic Acid. *Die Angew. Makromol. Chem.* **1981**, *93*, 189–198. [CrossRef]
20. Sun, R.; Liu, B.; Li, B.G.; Jie, S. Palladium(II)@Zirconium-Based Mixed-Linker Metal–Organic Frameworks as Highly Efficient and Recyclable Catalysts for Suzuki and Heck Cross-Coupling Reactions. *ChemCatChem* **2016**, *8*, 3261–3271. [CrossRef]
21. Yildiz, C.; Kutonova, K.; Oßwald, S.; Titze-Alonso, A.; Bitzer, J.; Bräse, S.; Kleist, W. Post-Synthetic Modification of DUT-5-Based Metal Organic Frameworks for the Generation of Single-Site Catalysts and Their Application in Selective Epoxidation Reactions. *ChemCatChem* **2020**, *12*, 1134–1142. [CrossRef]
22. Gotthardt, M.A.; Grosjean, S.; Brunner, T.S.; Kotzel, J.; Gänzler, A.M.; Wolf, S.; Bräse, S.; Kleist, W. Synthesis and Post-Synthetic Modification of Amine-, Alkyne-, Azide- and Nitro-Functionalized Metal–Organic Frameworks Based on DUT-5. *Dalton Trans.* **2015**, *44*, 16802. [CrossRef]
23. Qian, W.; Huang, W.; Cong, Y.; Li, F. Selective Oxidation of Benzyl Alcohols Catalyzed by UiO-67-Sal-$CuCl_2$ in Air. *Chem. J. Chin. Univ.* **2019**, *40*, 1178–1183.
24. He, L.; Wang, R.-D.; Wang, S.; Zhu, R.-R.; Li, Z.; Wu, Y.-Y.; Ma, J.; Du, L.; Zhao, Q.-H. An AIE Material with Time-Dependent Luminescence Conversion Obtained by 2D Coordination Polymer Modification via Covalent Post-Synthetic Modification. *Dalton Trans.* **2021**, *50*, 16685. [CrossRef] [PubMed]
25. Olkhovik, V.K.; Vasilevskii, D.A.; Pap, A.A.; Kalechyts, G.v; Matveienko, Y.v; Baran, A.G.; Halinouski, N.A.; Petushok, V.G. Synthesis of New Polyconjugated Molecules with Biphenyl, Dibenzothiophene, Carbazole and Phenanthrene Units. *Arkivoc* **2008**, *9*, 69–93. [CrossRef]
26. Khansari, A.; Bryant, M.R.; Jenkinson, D.R.; Jameson, G.B.; Qazvini, O.T.; Liu, L.; Burrows, A.D.; Telfer, S.G.; Richardson, C. Interpenetration Isomers in Isoreticular Amine-Tagged Zinc MOFs. *CrystEngComm* **2019**, *21*, 7498. [CrossRef]
27. Deshpande, R.K.; Minnaar, J.L.; Telfer, S.G. Thermolabile Groups in Metal-Organic Frameworks: Suppression of Network Interpenetration, Post-Synthetic Cavity Expansion, and Protection of Reactive Functional Groups. *Angew. Chem.-Int. Ed.* **2010**, *49*, 4598–4602. [CrossRef]
28. Dikhtiarenko, A.; Olivos Suarez, A.I.; Pustovarenko, A.; García-Granda, S.; Gascon, J.; Suarez, A.I.O.; Pustovarenko, A.; García-Granda, S.; Gascon, J. Crystal Structure of 2,2′-Diamino-[1,1′-Biphenyl]-4,4′-Dicarboxylic Acid Dihydrate, $C_{14}H_{16}N_2O_6$. *Z. Krist.-New Cryst. Struct.* **2016**, *231*, 65–67. [CrossRef]
29. Groom, C.R.; Bruno, I.J.; Lightfoot, M.P.; Ward, S.C. The Cambridge Structural Database. *Acta Crystallogr. B Struct. Sci. Cryst. Eng. Mater.* **2016**, *72*, 171–179. [CrossRef]
30. Hylland, K.T.; Gerz, I.; Wragg, D.S.; Øien-Ødegaard, S.; Tilset, M. The Reactivity of Multidentate Schiff Base Ligands Derived from Bi- and Terphenyl Polyamines towards M(II) (M=Ni, Cu, Zn, Cd) and M(III) (M=Co, Y, Lu). *Eur. J. Inorg. Chem.* **2021**, *2021*, 1869–1889. [CrossRef]
31. Cheeseman, T.P.; Hall, D.; Waters, T.N. The Colour Isomerism and Structure of Some Copper Co-Ordination Compounds. Part XII. The Crystal Structure of NN′-(2{,}2′-Biphenyl)Bis(Salicylaldiminato)Copper(II). *J. Chem. Soc. A* **1966**, 1396–1406. [CrossRef]
32. Ababneh, T.S.; Al-Shboul, T.M.A.; Jazzazi, T.M.A.; Alomari, M.I.; Görls, H.; Westerhausen, M. Crystallographic and Computational Study of the Structure of Copper(II) 2,2′-Bis(2-Oxidobenzylideneamino)-4,4′-Dimethyl-1,1′-Biphenyl. *Transit. Met. Chem.* **2020**, *45*, 435–442. [CrossRef]
33. Heo, J.; Jeon, Y.-M.; Mirkin, C.A. Reversible Interconversion of Homochiral Triangular Macrocycles and Helical Coordination Polymers. *J. Am. Chem. Soc.* **2007**, *129*, 7712–7713. [CrossRef] [PubMed]
34. Kunert, R.; Philouze, C.; Berthiol, F.; Jarjayes, O.; Storr, T.; Thomas, F. Distorted Copper(Ii) Radicals with Sterically Hindered Salens: Electronic Structure and Aerobic Oxidation of Alcohols. *Dalton Trans.* **2020**, *49*, 12990–13002. [CrossRef] [PubMed]
35. Panther, T.; Baumann, U. Dinukleare Kupfer (II)-Komplexe Mit Chiralen Makrocyclischen Liganden Vom Schiff-Basen-Typ: Synthesen Und Strukturen Complexes with Macrocyclic Ligands. V Dinuclear Copper (II) Complexes with Chiral Macrocyclic Ligands of Schiff-Base Type: Synthes. *Synthese* **2001**, *627*, 238–243. [CrossRef]
36. Che, C.-M.; Kwong, H.-L.; Chu, W.-C.; Cheng, K.-F.; Lee, W.-S.; Yu, H.-S.; Yeung, C.-T.; Cheung, K.-K. Copper Complexes of Chiral Tetradentate Binaphthyl Schiff-Base Ligands: Syntheses, X-Ray Crystal Structures and Activity in Catalytic Asymmetric Cyclopropanation of Alkenes. *Eur. J. Inorg. Chem.* **2002**, *2002*, 1456–1463. [CrossRef]
37. Saito, M.; Sato, H.; Mori, Y.; Fukuda, Y. Structure and Enantio-Differentiating Behaviors of Nickel(Ii) Complexes with Chiral Schiff Base Ligands Derived from 1, 1′ Binaphthyl-2,2′-Diamine. *Bull. Chem. Soc. Jpn.* **2009**, *82*, 1266–1273. [CrossRef]
38. Wang, Y.; Stack, T.D.P. Galactose Oxidase Model Complexes: Catalytic Reactivities. *J. Am. Chem. Soc.* **1996**, *118*, 13097–13098. [CrossRef]
39. Addison, A.W.; Rao, T.N.; Reedijk, J.; van Rijn, J.; Verschoor, G.C. Synthesis, Structure, and Spectroscopic Properties of Copper(II) Compounds Containing Nitrogen–Sulphur Donor Ligands; the Crystal and Molecular Structure of Aqua[1,7-Bis(N-Methylbenzimidazol-2′-Yl)-2,6-Dithiaheptane]Copper(II) Perchlorate. *J. Chem. Society. Dalton Trans.* **1984**, 1349–1356. [CrossRef]
40. Holmes, R.R. Structure of Cyclic Pentacoordinated Molecules of Main Group Elements. *Acc. Chem. Res.* **1979**, *12*, 257–265. [CrossRef]
41. Holmes, R.R. Five-Coordinated Structures. In *Progress in Inorganic Chemistry*; Lippard, S.J., Ed.; John Wiley & Sons, Ltd.: Hoboken, NJ, USA, 1984; Volume 32, pp. 119–235, ISBN 9780470166338.
42. Pinsky, M.; Avnir, D. Continuous Symmetry Measures. 5. The Classical Polyhedra. *Inorg. Chem.* **1998**, *37*, 5575–5582. [CrossRef]

43. Sheldrick, G.M. Foundations and Advances SHELXT-Integrated Space-Group and Crystal-Structure Determination. *Acta Crystallogr. Sect. A* **2015**, *71*, 3–8. [CrossRef]
44. Sheldrick, G.M. Crystal Structure Refinement with SHELXL. *Acta Crystallogr. Sect. C* **2015**, *71*, 3–8. [CrossRef] [PubMed]
45. Spek, A.L. PLATON SQUEEZE: A Tool for the Calculation of the Disordered Solvent Contribution to the Calculated Structure Factors. *Acta Crystallogr. C Struct. Chem.* **2015**, *71*, 9–18. [CrossRef] [PubMed]
46. Spek, A.L. Biological Crystallography Structure Validation in Chemical Crystallography. *Acta Crystallogr. Sect. D* **2009**, *65*, 148–155. [CrossRef] [PubMed]
47. Bruno, I.J.; Cole, J.C.; Kessler, M.; Luo, J.; Momerwell, W.D.S.; Purkis, L.H.; Smith, B.R.; Taylor, R.; Cooper, R.I.; Harris, S.E.; et al. Retrieval of Crystallographically-Derived Molecular Geometry Information. *J. Chem. Inf. Comput. Sci.* **2004**, *44*, 2133–2144. [CrossRef]
48. MacRae, C.F.; Sovago, I.; Cottrell, S.J.; Galek, P.T.A.; McCabe, P.; Pidcock, E.; Platings, M.; Shields, G.P.; Stevens, J.S.; Towler, M.; et al. Mercury 4.0: From Visualization to Analysis, Design and Prediction. *J. Appl. Crystallogr.* **2020**, *53*, 226–235. [CrossRef]